Title

Modeling the effects of coastal wind- and wind–stress curl-driven upwellings on plankton dynamics in the Southern California current system

Authors

Macías, D
Franks, PJS
Ohman, MD
et al.

Publication Date

2012-06-01

DOI

10.1016/j.jmarsys.2011.11.011

Peer reviewed

Journal of Marine Systems 94 (2012) 107–119

Contents lists available at SciVerse ScienceDirect

Journal of Marine Systems

journal homepage: www.elsevier.com/locate/jmarsys

Modeling the effects of coastal wind- and wind–stress curl-driven upwellings on plankton dynamics in the Southern California current system

D. Macías [a,b,*], P.J.S. Franks [a], M.D. Ohman [a], M.R. Landry [a]

[a] Integrative Oceanography Division, Scripps Institution of Oceanography, University of California at San Diego, La Jolla, CA 92093, USA
[b] Departamento de Ecología y Gestión Costera, Instituto Andaluz de Ciencias Marinas (CSIC), 11510 Puerto Real, Spain

ARTICLE INFO

Article history:
Received 4 November 2010
Received in revised form 2 November 2011
Accepted 9 November 2011
Available online 13 December 2011

Keywords:
Biogeochemical models
Data-simulations comparison
U.S.A
California Current System
Southern California Bight
CALCOFI
CCE-LTER

ABSTRACT

We use a Nitrogen-Phytoplankton-Zooplankton-Detritus (NPZD) biogeochemical model implemented in a time-dependent box model scheme to simulate the temporal dynamics of the pelagic ecosystem in the Southern California Current System (SCCS). The model was forced by winds, sea surface temperature and light. Nutrient inputs to the modeled box were driven by coastal upwelling or upwelling due to wind-stress curl in order to assess the importance of each process in the temporal dynamics of the SCCS ecosystem. Model results were compared to the CalCOFI dataset, both in terms of climatological annual cycles and actual values. This comparison led to modifications of the basic model structure to better represent the coastal ecosystem, particularly phytoplankton growth and zooplankton mortality terms. Wind-stress curl-induced upwelling was found to be significant only in the offshore regions while coastal upwelling better represented the dynamics of the inshore areas. The two upwelling mechanisms work in synchrony, however, to bring nutrients to surface waters during the same time periods. Finally, the effect of low-frequency perturbations, such as those associated with the ENSO and NPGO, were assessed by comparing model results and data. Since the NPGO cycle largely impacts the SCCS through modifications of upwelling-favorable winds, its effects were well represented in the model results. In contrast, ENSO responses were poorly captured in the simulations because such perturbations alter the system by changing surface water mass distributions via mechanisms that were not included in the model forcing.

1. Introduction

The California Current System (CCS) comprising the eastern boundary current of the North Pacific Gyre extends more than 15° of latitude over a range of temporally and spatially variable environments with subpolar to subtropical influences. Eastern boundary currents are among the most productive marine coastal environments in the world (Carr, 2002), providing the base for food webs that support some of the most economically important fisheries. The high biological productivity in the CCS is primarily fueled by the supply of nutrients from wind-driven upwelling as a result of the prevailing equatorward winds that push the near-surface waters offshore through Ekman transport, causing nutrient-rich waters from mid-depths to upwell to the surface (e.g. Murphree et al., 2003; Wooster and Reid, 1963).

In the northern CCS, along the relatively straight and north–south oriented coastline of Washington and Oregon, strong seasonal reversals in winds drive dramatic annual cycles in onshore and offshore currents, hydrographic properties and productivity (Hickey, 1979; Lynn and Simpson, 1987). Seasonal and interannual variabilities in productivity are closely tied to wind-driven coastal upwelling, with the offshore density front and equatorward jet responding rapidly to fluctuations in the strength of upwelling-favorable (southward) winds (Huyer and Smith, 1985; Strub and James, 2000). However, upwelling is not a spatially uniform process. Certain regions are more conducive to upwelling (Schwing and Mendelssohn, 1997), and local characteristics (topography, bathymetry, hydrography) can strongly modify the seasonal production patterns expected from the annual wind cycle on a regional scale (e.g. Henson and Thomas, 2007; Hickey and Banas, 2008). It is also known that several climatic phenomena influence the CCS on interannual scales, such as the strength and position of the Aleutian Low atmospheric pressure system (Rebstock, 2003) represented by the magnitude of the Pacific Decadal Oscillation index (PDO) (Mantua et al., 1997). Especially in the northern CCS, the phase and magnitude of the PDO index has been found to be correlated with fluctuations in standing stocks of phytoplankton (Thomas et al., 2009), zooplankton (Mackas et al., 2006), and fishes (Mantua et al., 1997).

In contrast to the northern CCS, the mechanisms connecting physical forcings and biological productivity are less clear in the southern sector of the California Current System (SCCS). Bathymetry and topography are complex in the area south of Point Conception (ca. 35°N) down to Baja California. Notably, the sharp eastward bend in the coastline at Point Conception (which creates the Southern California Bight (SCB)) establishes a wind gradient with an offshore maximum when southerly upwelling-favorable winds blow down the coast. Also, local wind stress

* Corresponding author at: Departamento de Ecología y Gestión Costera, Instituto Andaluz de Ciencias Marinas (CSIC), 11510 Puerto Real, Spain.
E-mail address: diego.macias@icman.csic.es (D. Macías).

0924-7963/$ – see front matter © 2011 Elsevier B.V. All rights reserved.
doi:10.1016/j.jmarsys.2011.11.011

at the coastline is generally weaker and without the pronounced seasonal directional changes of the northern region. Temporal physical dynamics of the SCCS are further complicated by currents that vary with the local surface winds (Allen, 1980).

Plankton dynamics in the SCCS have been well documented (Allen, 1941; Hayward and Venrick, 1998) but are still not well understood. One of the main points of debate is the extent to which coastal upwelling is responsible for the annual plankton cycle (as it is in the northern CCS) since regular coastal upwelling is limited to a small region around Pt. Conception (Fig. 1) (Hickey, 1979; Lynn and Simpson, 1987). Di Lorenzo (2003) has noted, however, that isopycnals generally tilt upward along the coast during the upwelling season, forced by winds in the SCB. While upwelling-favorable winds relax close to shore during summer, they are still strong offshore near the continental slope. This positive gradient generates wind-stress curl and offshore upwelling. The relative contributions of the two upwelling processes to plankton production in the SCCS are poorly known. Recent estimates suggest, however, that wind-stress curl, though of lesser intensity than coastal upwelling, could provide half or more of the upwelling transport within the CCS because it affects a much larger surface area (Pickett and Paduan, 2003; Rykaczewski and Checkley, 2008).

Another important feature of the annual production cycle in the SCCS is its response to remote forcing by climatic patterns, one of the most significant on interannual scales being the El Niño-Southern Oscillation (ENSO) (Bograd and Lynn, 2001). Decreased biological productivity is observed in the SCCS during El Niño events, generally with an opposite response during La Niña conditions (Chavez et al., 1998). An additional potentially influential climatic oscillation in the region is the North Pacific Gyre Oscillation (NPGO) described by Di Lorenzo et al. (2008). This climatic pattern emerges as the 2nd dominant mode of sea surface height variability in the Northeast Pacific and is well correlated with upwelling intensity and primary production along the California coast.

With >60 years of time-series sampling in the SCCS, the California Cooperative Oceanic Fisheries Investigations (CalCOFI) provide a rich data set for understanding seasonal patterns and long-term trends in the region (Bograd et al., 2003; Lavaniegos and Ohman, 2007). Here, we attempt to synthesize the data using a coupled physical-biological model (c.f., Riley, 1941). Simulating the small spatial scales, rapid time-varying processes and strong mesoscale features of coastal systems (e.g., Moisan et al., 2004) has progressed rapidly in the last decade with the increase in computer technologies, improved methods for computational fluid dynamics, improved knowledge of ocean circulation and biogeochemical dynamics, and large increase in availability of remotely sensed data for model forcing and validation (Moore et al., 2004).

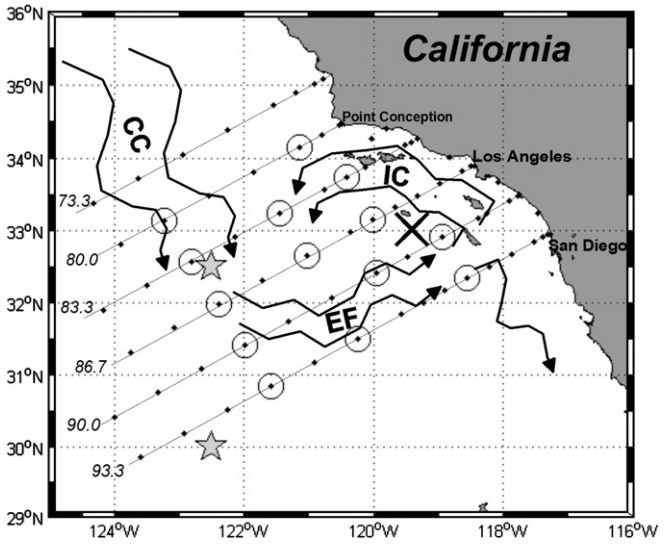

Fig. 1. The Southern California Current System. Black dots are the CalCOFI grid stations. Encircled stations are used for climatological comparison. Black cross show the location of the coastal upwelling index (CUI) estimate, and gray stars are the positions where wind-stress curl was calculated. The main circulation features are also shown schematically: the California Current (CC), the Ensenada Front (EF) and the Inshore Countercurrent (IC).

Our approach to simulating these highly dynamic areas is to reduce complexity to minimum levels by using integrative representations. Thus, in the present work we simulate ecosystem dynamics of the SCCS with a NPZD model using a time-dependent box model framework of the surface ocean. Nutrient input to the modeled box is forced by either coastal or wind-stress curl-driven upwelling. This box-model physical framework has been applied successfully to simulate coastal upwelling systems in previous studies (e.g., Ianson and Allen, 2002; Olivieri and Chavez, 2000). Its simplicity greatly reduces the computational cost, allowing a more thorough analysis of the simulation results and more extensive comparison with observational data.

The biogeochemical model is based on Fasham et al. (1990), which was initially developed to simulate the seasonal cycle of nutrients and primary production at Station S off Bermuda and includes a simplified microbial loop represented by heterotrophic bacteria. This general formulation has been used in many local, regional and basin-scale applications with considerable success (e.g., Fasham, 1995; Sarmiento et al., 1993; Toggweiler and Carson, 1995).

In the present study, results of the model are compared to climatological and actual values from the CalCOFI grid to evaluate (i) the relative importance of upwelling processes (coastal versus wind-stress curl) and (ii) the potential of this simple approach to predict the conditions of the SCB under different climate scenarios, including ENSO cycles and NPGO variations.

2. Material and methods

Our model is only time dependent, with a "virtual box" represented by mean parameter values of the upper 50 m water in the SCB. The horizontal dimension of the box is approximately equal to the internal Rossby radius of deformation in the area, calculated to be around 10 km (e.g., Franks, 1992).

Two different sets of simulations are performed, one using coastal upwelling forced by Ekman pumping and the other using wind-stress curl-induced upwelling as the main external forcing to the model (see detailed description below). Each simulation represents 42 year period, from 1967 to 2008, the length of the available upwelling time-series. Each simulation was initiated after a spin-up run of 10 years i.e., the model was run during the first 10 years of the available upwelling forcing using as initial values the mean of all model constituents for the region available in the literature. The ecosystem final state after these 10 years run was used as the initial condition for the 42-year run. Model equations were solved using the *ode45* function in Matlab®, which adjusts the time step to ensure that the maximum difference between consecutive integrations is of order 10^{-6}. The output was collected and stored for each 14.4 minutes of simulation, essentially breaking each day into 100 time steps.

We assume that the water input to the modeled box (computed as described below) only contains nitrate, with the concentrations of all other constituents of the ecosystem being zero. The upwelled water with associated nutrients is considered to be immediately mixed and homogeneously distributed throughout the entire box neglecting any spatial heterogeneity. To conserve volume, an equal amount of water to that introduced by upwelling leaves the modeled box at each time step. This outflowing water has the characteristics of the box waters, with identical concentrations of all constituents of the ecosystem, both living and nonliving.

2.1. Nutrient input to the modeled box

2.1.1. Coastal upwelling

Nutrient input from coastal upwelling is calculated from the California Upwelling Index (CUI), which gives offshore (positive) or onshore (negative) estimates of water transport (m^3/s) integrated over 100 m of shoreline. CUI values, calculated at 15 locations along the western American coast by the Pacific Fisheries Environmental Laboratory (PFEL), were downloaded from the PFEL web database (http://www.pfeg.noaa.gov/products/las.html). The time series represents the effect of the local geostrophic winds (e.g., Smith et al., 2001; Wainwright et al., 2007) derived from six-hourly synoptic and monthly mean fields of surface atmospheric pressure. The pressure fields are provided by the U.S. Navy Fleet Numerical Meteorological and Oceanographic Center (www.fnmoc.navy.mil) at Monterey, California (Bakun, 1973). Details regarding the theory and methods used for these transport estimates are given by Schwing et al. (1996). The different temporal resolutions of the CUI time-series available from PFEL range from 6-hourly data to monthly integrated values.

For the present work, both daily and monthly CUI data from 33°N (black cross in Fig. 1) were used to quantify the effects of the different forcing resolutions on the model's behavior. Both time series were adjusted to give the same integrated amount of water input over the 42-year simulations. Also, to determine if both upwelling time series were equivalent from a statistical point of view, a Singular Spectral Analysis was applied following the protocols described by Macías et al. (2007).

The combination of the CUI values and the Rossby radius of deformation described above gave vertical velocities ranging from −1 (downwelling) to 7 m d^{-1}, which fall within the range of values of 1–10 m d^{-1} for coastal upwelling systems (Smith, 1968).

To calculate nutrient inputs, the flux values of the CUI were multiplied by the nitrate concentration at 60 m (e.g., Castro et al., 2002) using the mean value of 9 μM reported for the near-shore area by Mantyla et al. (2008). As noted above, the nutrient input was considered to be immediately mixed into the system, neglecting spatial heterogeneity.

To test whether the CUI estimates at 33°N could be considered representative of the SCCS region, a correlation analysis was done with all the CUI time series available, from 21°N to 60°N (not shown). As expected, the correlations diminished with distance both north and south of the study location (33°N). However, the correlation coefficient was above 0.7 for the SCCS (from 30°N to 36°N), meaning that the selected CUI adequately represented the coastal upwelling index for the entire SCCS region.

2.1.2. Wind-stress curl-driven upwelling

Wind-stress data were downloaded from the PFEL web site as a reanalysis of the National Centers for Environmental Prediction (NCEP) surface wind fields (base period 1967–2008; horizontal resolution of 2.5°; (Kistler et al., 2001). Monthly data (in Newtons m^{-2}) were taken from 1967 to 2008 at 20 locations between 22.5°N and 32.5°N and 120°W and 127.5°W. These data were used to compute the associated wind-stress curl along three longitudinal lines (located at 120°W, 122.5°W, 125°W, and 127.5°W from 27.5°N to 32.5°N) by computing the horizontal divergence/convergence between nearby positions in the grid. Horizontal divergence was assumed to be compensated by vertical ascent of deep waters to conserve mass. The wind-curl time series were nearly identical in the three most offshore lines, so the one located at 122.5°W (gray stars in Fig. 1) was selected as representative of this outer region. In contrast, wind-stress curl on the inner line (at 120°W) was predominantly associated with downwelling during the entire available time-series (not shown).

As discussed further below, the coarse resolution in space and time of this wind dataset will likely lead to underestimation of the associated wind-stress curl; however, it is the longest available record of wind forcing in the region and the only one comparable (in duration) to the coastal CUI.

Mean nitrate concentration at 60 m from the outer stations of the CalCOFI lines (mean = 3 μM, SD = 2.84) was used as the deep concentration entrained by the wind-stress curl. The nitrate flux was, calculated by multiplying the vertical water velocity computed by the wind-stress curl times this deep nitrate concentration. This nutrient input was assumed to be homogeneously mixed within the simulated box.

2.2. Sea surface temperature (SST) and light

The other external forcings to the model were the annual cycles of SST and incident light. SST data were obtained from the World Ocean Atlas 2001 (WOA01), which provides a time series of monthly temperatures from 1950 to 2001. However, this time series is not complete, nor does it cover the entire simulation time (which ends in 2008). Missing values within the series were replaced by the climatological values for the missing months (i.e., the monthly mean values from the time series).

The astronomical equations proposed by Brock (1981) and the cloud cover model by Smith and Dobson (1984) were used to compute sea surface irradiance (I_o) using the time of year, latitude and cloud cover (set at a fixed mean value of 3 oktas).

2.3. Ecosystem model

The ecosystem model used is a simple, N-based, NPZD model as originally designed by Fasham et al. (1990), with refinements in the formulations of some processes and parameters (see Table 1 and Appendix 1). The equations for the seven different components of the model include phytoplankton (Eqs. (A.1) to (A.10)), zooplankton (Eqs. (A.11) to (A.15)), bacteria (Eqs. (A.16) to (A.20)), detritus (Eqs. (A.21) and (A.22)), nitrate (Eq. (A.23)), ammonium (Eq. (A.24)) and dissolved organic nitrogen (DON) (Eq. (A.25)).

For phytoplankton, the main modification of the Fasham et al. (1990) model was for maximum growth rate, which was fixed in the original model and here is temperature dependent (Eq. (A.3)). Temperature-dependence of phytoplankton maximum growth rate was implemented as a modification of Eppley et al. (1969), to align with field measured rates (Landry et al., 2009) by dividing calculated rates from the original relationship by 3.7, as shown in Eq. (A.3).

For zooplankton, the main modifications were in the grazing and mortality expressions. For grazing, a density-dependent Holling Type III expression was used to modulate the maximum rate of zooplankton consumption of phytoplankton, bacteria and detritus (Eqs. (A.7), (A.12) and (A.13); e.g., Fasham, 1995; Fennel et al., 2006). Mortality was expressed by two Eqs. (A.14) and (A.15), one representing the natural mortality rate (Eq. (A.14)) and the other (Eq. (A.15)) accounting for a "predation mortality" which acts as a model closure (following Olivieri and Chavez, 2000; c.f. Ohman and Hirche, 2001). For the rest of the model's constituents, the expressions used were the same as developed by Fasham et al. (1990).

2.4. Field data

The spatial domain, and certain measurements and techniques of the CalCOFI cruises have changed with time (Bograd et al., 2003). In our simulation region, however, at least five lines have been sampled consistently during the entire time-series: lines 80.0, 83.3, 86.7, 90.0 and 93.3 (transects in Fig. 1). To compare with model results, we used field data from a set of 14 stations distributed along those five lines (encircled stations in Fig. 1) to average over north–south and offshore-inshore variability of the SCCS.

Hydrographic data were downloaded from http://www.calcofi.org/data/btldata.html. Routine CalCOFI station occupations since April 1993 have deployed a SeaBird CTD instrument with a 24-place

Table 1
Model variables and parameter values.

Symbol	Name	Value	Source
P	Phytoplankton state variable	State variable	
Z	Zooplankton state variable	State variable	
B	Bacteria state variable	State variable	
D	Detritus state variable	State variable	
Nn	Nitrate	State variable	
Nr	Ammonia	State variable	
Nd	DON	State variable	
Ω	Fraction of primary production exuded as DON	0.05	Fasham et al., 1990
λ	PAR fraction of solar radiation	0.43	Fasham et al., 1990
a	Air-sea albedo	0.05	Fasham et al., 1993
oktas	Clould cover (0–8)	Default: 3	Standard value
k_w	Attenuation coefficient of water	0.04 m^{-1}	Fasham et al., 1990
I_0	Incident light	1000 (W/m^2)	Standard value
Depth	Depth of the modeled box	50 (m)	Standard value
Vp	Phytoplankton maximum growing rate	Temperature dependent (d^{-1})	Eppley, 1972 (scaled to Landry et al., 2009
α	Initial slope of P-I curve	0.05 $(Wm^{-2})^{-1}$ d^{-1}	Fasham et al., 1993
k_1	Half saturation constant for nitrate uptake	0.5 mMol N m^{-3}	Fasham et al., 1990
k_2	Half saturation constant for ammonium uptake	0.5 mMol N m^{-3}	Gruber et al., 2006
mu_1	Maximum phytoplankton mortality rate	0.024 d^{-1}	Gruber et al., 2006
k_c	Self-shading coefficient	0.03 m^2 $(mMol\ N)^{-1}$	Fasham et al., 1990
γ	Fraction of PP exuded as DON	0.05	Fasham et al., 1990
psi	Nitrate uptake inhibition (by ammonium)	1.5 $(mMol\ N)^{-1}$	Fasham et al., 1990
g	Maximum zooplankton ingestion rate	0.6 d^{-1}	Fennel et al., 2006
β	Zooplankton ingestion efficiency	0.75	Fasham et al., 1990
mu_2	Zooplankton maximum excretion rate	0.1 d^{-1}	Fasham et al., 1990
mu_5	Zooplankton maximum mortality rate due to consumption	0.05 $(mMol\ N\ m^{-3})^{-1}$ d^{-1}	Olivieri and Chavez, 2000
k_3	Zooplankton ingestion half saturation constant	3.0 $(mMol\ N\ m^{-3})$	Olivieri and Chavez, 2000
δ	Fraction of zoop. losses to DON	0.2	Fasham et al., 1993
Vb	Bacterial maximum growth rate	2.0 d^{-1}	Fasham et al., 1990
mu_3	Bacterial maximum loss rate	0.05 d^{-1}	Fasham et al., 1990
k_4	Bacterial uptake half saturation constant	0.5 mMol N m^{-3}	Fasham et al., 1990
n_u	DON:ammonium uptake ratio	0.6	Fasham et al., 1990
mu_4	Detritus maximum breakdown rate	0.05 d^{-1}	Fasham et al., 1990
S_D	Detritus sinking rate	5 m d^{-1}	Fasham et al., 1990
k_5	Half saturation constant of phytoplankton mortality	0.2 $(mMol\ N\ m^{-3})$	Popova et al., 1997
p_1	Zooplankton preference for phytoplankton	0.5	Fasham et al., 1990
p_2	Zooplankton preference for bacteria	0.25	Fasham et al., 1990
p_3	Zooplankton preference for detritus	0.25	Fasham et al., 1990

rosette of 10-L PVC Niskin bottles. Casts were routinely made to 525 m depth, bottom depth permitting.

Dissolved silicic acid, phosphate, nitrate and nitrite concentrations were determined at sea using an automated analyzer (Atlas et al., 1971), following procedures similar to those described in Gordon et al. (1993). Samples for fluorimetric determination of chlorophyll-*a* (Chla) and phaeopigment concentrations were taken only in the upper 200 m. Further details of the standard sampling and analytical procedures, along with all data and derived variables, can be found in the CalCOFI data report series (e.g., Scripps Institution of Oceanography, 2002). For model testing, we used basic information of physical (i.e., temperature) and biogeochemical (i.e., nitrate and chlorophyll concentrations) properties from the 0–50 m depth range at each sampling station.

Since phytoplankton biomass was estimated from extracted Chla, a N:Chla conversion ratio was needed to compare with the model results. This ratio varies naturally by nearly one order of magnitude, depending mainly on light and nutrient availability (e.g. Geider et al., 1998). Since the study region is a coastal area with moderately high nutrient concentrations (at least during certain seasons), a N:Chla ratio of 5 (mg/mg) was chosen. This is within the range reported for eutrophic (Laws and Bannister, 1980; Osborne and Geider, 1986) or coastal environments (Fennel et al., 2006) and is also within the range used by Gruber et al. (2006) for central California and close to the upper limit of Chla:C ratio reported by Li et al. (2010) for Point Conception (assuming a Redfield C:N ratio). Li et al. (2010) found a progressive onshore-to-offshore decrease of the Chla:C ratio. The N:C ratio of phytoplankton would also be expected to decrease with nutrient limitation in the offshore oligotrophic waters. Given the compensatory effects of these trends on N:Chla ratios, here we used the constant ratio (=5) for simplicity and to avoid uncertainties associated to the C:N conversion.

Zooplankton data were more difficult to obtain in a format directly comparable to the model output (N concentration). This information is usually available as numerical abundance or, more commonly, as bulk biomass (e.g., displacement volume). However, Lavaniegos and Ohman (2007) provide basic information for calculating carbon contents of meso- and macrozooplankton in the SCCS based on detailed taxonomic analyses. We use their data from at least two complete annual cycles, corresponding to the cold and warm phases of the PDO, to generate a mean annual cycle in nitrogen units, applying the Redfield ratio (Redfield, 1934) to the carbon data. This climatologic year is the one used to compare with the model simulations.

However, this annual cycle is constructed using data from only two years (see Fig. 14 in Lavaniegos and Ohman, 2007). In order to confirm whether the annual cycle described in their data was a consistent feature in time, we also used macrozooplankton (>505 μm) displacement volume (DV) from CalCOFI cruises (http://oceaninformatics.ucsd.edu/datazoo/data/). Data from nighttime net tows (19:00 to 06:00) collected from 1969 to 2008 on the southernmost 5 lines of the CalCOFI grid (Fig. 1) were transformed into ash free dry mass (AFDM) using the conversion factors reported by Ohman and Wilkinson (1989). This AFDM was then transformed assuming that 45% was C (Ohman, pers. comm.) and converted to N using the Redfield ratio (Redfield, 1934).

Direct comparison of DV-derived biomass and those computed from the Lavaniegos and Ohman (2007) relationship yields a high correlation coefficient ($r > 0.8$) and a slope close to one ($m = 0.7$). This suggests that the annual cycle of zooplankton biomass is coherent throughout the

time series. However the DV-derived data should not be used for direct comparison with the model results due to a shift in community composition (mainly a long-term decline in pelagic tunicates) that affected the biovolume:carbon ratio (Lavaniegos and Ohman, 2007).

2.5. Model-data comparison

We ran the model forced with the 42 available years of wind-derived upwelling (daily CUI, monthly CUI and wind-stress curl), creating three time series of ecosystem response. From these time series, we generated climatologic cycles of the different variables (N,P,Z).To compare with the three model runs, CalCOFI data at each station included in the comparison (Fig. 1) were used to calculate the climatologic cycles for each location. For the general comparison between model and data presented in Fig. 4, all field data were merged into a unique time-series, creating a common climatologic cycle of each variable for the entire SCCS.

3. Results

3.1. Model results

3.1.1. Coastal upwelling

The model was run for the 42 years of available data of CUI (both daily and monthly). To make both simulations comparable, both CUI time-series were adjusted to provide exactly the same amount of upwelled water during the simulation time (Table 2). Simulated phytoplankton and zooplankton biomass induced by the daily and monthly CUI forcing showed clear annual cycles of both trophic levels, with values peaking in spring/summer and lower biomass during fall and winter (Fig. 2). The shapes of the time series were similar for both monthly and daily upwelling indices. The average outflow of P and Z biomass computed for these two simulations was 1.49% of the total biomass within the modeled box with maximum values around 4% during spring (not shown).

In both cases, the total biomass of phytoplankton and zooplankton was dependent on the total input of nutrients forced by upwelling. The greater the flux of nutrient to the euphotic layer, the larger the biomass concentration. However, despite the similarities of the results obtained with the two upwelling estimates, there were significant (t-test, $p<0.01$) differences in the total biomass obtained with the two forcings (Table 3). On average, summed phytoplankton and zooplankton biomass was 6.5% higher in simulations forced by the daily CUI, although total nutrient input was exactly the same in both simulations.

3.1.2. Wind-stress-curl upwelling

Simulations performed with upwelling induced from wind-stress curl do not show an annual cycle each year (Fig. 3). However, when peaks in phytoplankton and zooplankton biomass occurred, they were generally during spring/early summer, sometimes with secondary maxima during fall. It is also noteworthy that biomass concentration was only an order of magnitude smaller for upwelling driven by wind stress curl compared to that generated from coastal upwelling (Figs. 2 and 3), while water flux (and nutrients) into the modeled box are between 4 and 3 times lower (Table 2).

Table 2
Integrated values mean and standard deviation of the fluxes into the modeled box calculated for the three different upwelling indexes.

	Total flux (m^3)	Mean flux ($m^3\ s^{-1}$)	Standard deviation ($m^3\ s^{-1}$)
Daily CUI	$1.14*10^{11}$	86.13	85.47
Monthly CUI	$1.14*10^{11}$	84.14	68.40
Wind-stress curl	$3.202*10^{7}$	0.097	0.0778

3.2. Model-field data comparison

3.2.1. Climatological cycles

Pooled data from the different stations in the SCCS (encircled stations in Fig. 1) were used to compute climatological values of the different variables during the simulation period (black dots in Fig. 4). The obvious pattern observed in these climatological-pooled data was a phytoplankton bloom in spring following the increase in the upwelling intensity and surface nitrate concentration. A few weeks later, there was a corresponding increase of zooplankton biomass, which contributed (along with nutrient depletion) to the decline of the phytoplankton bloom. A secondary phytoplankton bloom can be seen in June/July, when zooplankton biomass declined and nutrient concentrations again supported net positive growth of the phytoplankton community.

Climatologic trends are well reproduced by the model for nitrate, phytoplankton and zooplankton when CUI (solid black and gray lines in Fig. 4) forced the rate of external nutrient supply to the system (see insets in Fig. 4A, B and C). The slopes of the linear regressions between the model estimates and data values were close to 1.0 ($m=0.68$–0.88 in all cases, except for nitrate computed with the monthly CUI which has $m=0.4$). It is also noteworthy that the correlation coefficient was usually higher ($r=0.87$ for nitrate; $r=0.81$ for phytoplankton and $r=0.87$ for zooplankton) and more significant ($p<0.01$) when the model was forced by daily CUI (black line) compared to the monthly CUI values (gray line).

The most obvious mismatch between the climatological cycles of data and model occurred for the summer/fall values of zooplankton biomass (Fig. 4c). The data show a sharp decline in zooplankton biomass in mid-summer, with low biomass remaining through the end of the year while predicted values almost double the observed in the second half of the year and are well outside the confidence intervals calculated for the field data.

Wind-stress curl-driven upwelling in the model forced a much smaller flux of nitrate into the upper layer than coastal upwelling (Fig. 4a), but the shape of the climatological cycle was quite similar to the one presented by the pooled data. As noted, planktonic biomass (both phytoplankton and zooplankton) simulated using only the wind-stress curl upwelling was at least one order of magnitude lower than the observations (Fig. 4b and c). However, the general shapes of the climatological cycles were still similar to those observed in the data, with higher values in spring and low the rest of the year. In this case, the correlation coefficients of the regressions between observations and simulations were lower than with the CUI (insets in Fig. 4), and the slopes of those regressions were much smaller than 1 ($m=0.001$ for phytoplankton and $m=0.0003$ for zooplankton).

It is also possible to compare climatological cycles at each station of the CalCOFI grid with those predicted by the different model runs (Fig. 5). In Fig. 5, only those correlation coefficients corresponding to statistically significant ($p<0.01$) slopes above 0.4 are included, as the model needs not only to reproduce the temporal behavior (given by the r^2) but also the range of values (represented by the slope). Background gray levels in this figure correspond to the r^2 values while isopleths represent the slopes of the linear fits between model and data. It is clear that maximum correlation values occur at the coastal stations where the slope values are closer to one in the simulation forced by daily CUI.

For the model forced by upwelling associated with the wind-stress curl (lower panels of Fig. 5), higher correlations in terms of r^2 and m were found in the southwestern regions of the CalCOFI grid, presenting an almost complementary distribution with respect to the pattern for CUI forcing.

3.2.2. Interannual variability

To compare the model phytoplankton output to the observed phytoplankton data, three different time windows were selected during periods representing different climatic conditions. The first window was

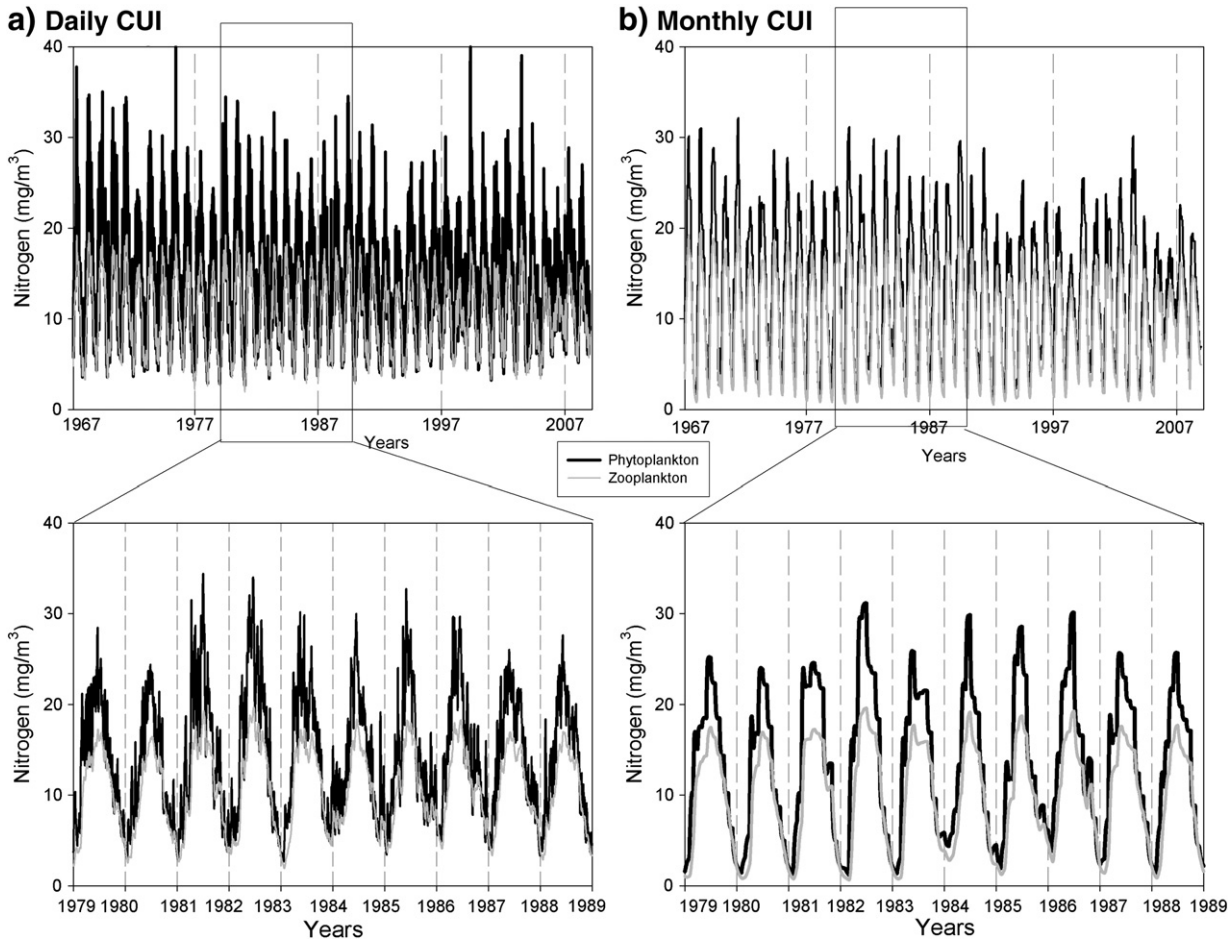

Fig. 2. Time series of phytoplankton (black line) and zooplankton (gray line) N biomass during 42 years of model simulation (upper panel) and during a central decade (lower panel) based on forcing by daily CUI (left graphs) and monthly CUI (right graphs).

2000–2004, characterized by the absence of important disturbances of the system (such as major El Niño events) and positive values of the NPGO (Fig. 6 left panels). The spatial distributions of r^2 during these 'neutral' years were similar to those observed with the climatological cycles (compare Figs. 5 and 6), with the CUI better simulating the inner part of the SCCS while the wind-stress curl-induced upwelling better represents the offshore region. It is also noteworthy that squared correlation coefficients for the actual data (Fig. 6) were roughly half the values obtained when compared with the climatological cycles (Fig. 5).

A second time window, 1995–1999, included one of the most energetic ENSO events of the last decades and still positive values of the NPGO. Substantial differences relative to the neutral years are evident, as correlation coefficients dropped below 0.1 for all stations for both types of upwelling forcing.

A final comparison was made using the 1993–1994 years as representative of the negative phase of the NPGO and with no El Niño perturbation (right panels of Fig. 6). The distributions of the correlation values were quite similar to those observed in the climatological comparison (Fig. 5) and during 2000–2004 (left panels of Fig. 6). The absolute values of r^2 were low due to the small number of observations available during 1993–1994.

Table 3
Integrated values (over time) of phyto- and zooplankton biomass (mg N/m^3) using the daily and monthly CUI. % Differences are computed as 100*(daily − monthly)/daily.

CUI series	Σ Phytoplankton biomass	Σ Zooplankton biomass	Σ Total biomass
Daily	$4.28*10^5$	$3.25*10^5$	$7.53*10^5$
Monthly	$4.06*10^5$	$2.97*10^5$	$7.07*10^5$
Difference	**5.14%**	**8.61%**	**6.11%**

4. Discussion

A very simple physical-biological model is able to simulate with reasonable statistical significance the climatological behavior of a complex ecosystem such as the SCCS. This is true for both nutrient and phytoplankton, as well as for zooplankton biomass, which tends to be more difficult to reproduce in models. However, some key modifications had to be made to the model to achieve good model-data comparisons.

4.1. Modifications to the model

The modifications to the original model structure focused on two main aspects: the effect of temperature on phytoplankton growth rate, and the formulation of the grazing and mortality terms of the zooplankton.

4.1.1. Temperature effect on phytoplankton growth

There were significant differences in model behaviors when using the original Eppley function for the temperature response of phytoplankton growth, as opposed to the scaled response developed here from data of Landry et al. (2009). The differences were mainly in the amount of nitrogen in the modeled box. When the original function was used, the average amount of free nitrate in the model was considerably lower than observed (difference of one order of magnitude) due to the much more rapid uptake by phytoplankton. When the growth rate was scaled to the experimentally measured values, the amount of nitrate was much closer to the data (Fig. 4a). Phytoplankton and zooplankton biomass were not greatly affected, remaining close to values in field data independent of the phytoplankton growth expression used. It is quite clear

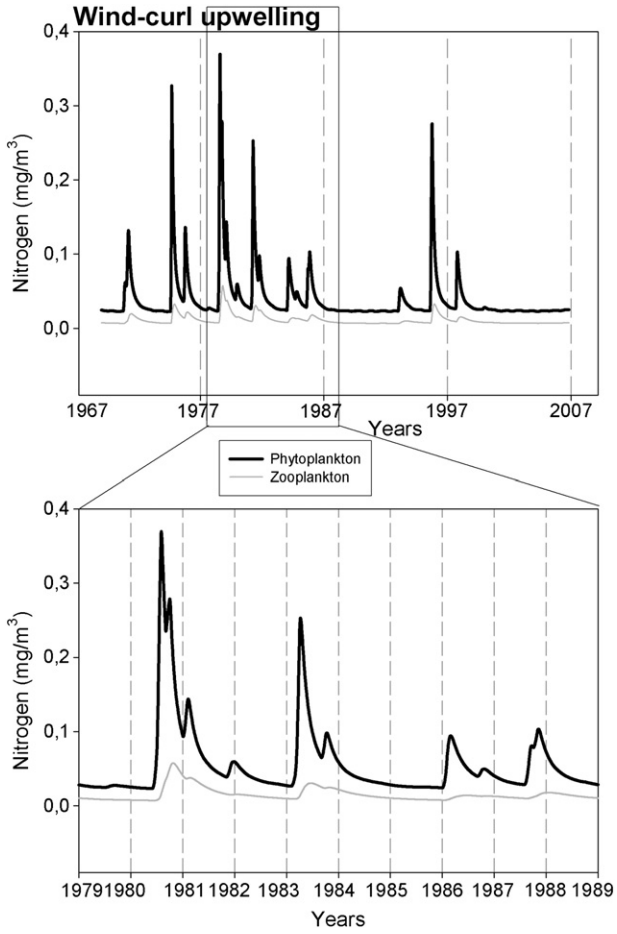

Fig. 3. Time series of phytoplankton (black line) and zooplankton (gray line) N biomass during 42 years of model simulation (upper panel) and during a central decade (lower panel) based on forcing by the wind stress curl.

that, at least for the SCCS, the use of field-derived estimates of phytoplankton growth rates is fundamental to obtaining an adequate representation of nitrate concentration in the surface layer.

However, even with the modification of the phytoplankton growth rate, climatological values of modeled nitrate were lower (5% for daily CUI and 35% for monthly CUI) than the observed concentrations (Fig. 4a). One of the likely reasons for these discrepancies is the highly simplified model structure which only consider a single phytoplankton type, do not include iron limitation (which is commonly observed in the field; Hopkinson and Barbeau, 2008; King and Barbeau, 2007), and has only a basic expression for ammonium competition. Boundaries conditions for model simulations (cloud cover, deep nutrient concentration and wind forcing resolution) could also be part of the reasons for the observed discrepancies.

4.1.2. Zooplankton cycles

Previous work by Gruber et al. (2006) has shown that better representations of plankton observations in the Monterey Bay coastal region were achieved when grazing parameter values and the mortality formulation of the zooplankton compartment in Fasham et al. (1990) were modified. The zooplankton community in the SCCS is very different from that in the Central North Atlantic for which the original model was developed, and the original zooplankton mortality function gave unrealistic cyclical behavior under nutrient-rich conditions (Steele and Henderson, 1992). Here, the mortality function was changed to a squared expression (Eq. (A.15)), as recommended by Steele and Henderson (1981) and as used by Fasham (1995) and McGillicuddy et al. (1995) for the same purpose. Ohman and Hirche (2001) provided field evidence supporting this density-dependent mortality of zooplankton. In addition, the grazing expressions (Eqs. (A.7), (A.12) and (A.13)) were changed to a Holling-type III functional response as proposed by Olivieri and Chavez (2000) for the northern CCS. Introducing these model refinements eliminated the limit cycles from the model simulations and improved the fit with the observations, giving further support to their necessity when modeling coastal environments, at least in the CCE region.

With these modifications, the magnitude and timing of the zooplankton blooms were fairly well reproduced by the model although large differences between model and observation were observed at the end of summer and through the fall (Fig. 4c). This can likely be attributed to a shift in zooplankton community size structure, which is not adequately represented in the field data. Lavaniegos and Ohman (2007) only identified zooplankton individuals larger than 0.5 mm for constructing the annual zooplankton cycles used for comparison with the model simulations. Larger organisms typically dominate biomass during the first half of the year, feeding on larger phytoplankton taxa, which are more abundant during the bloom phase (Vargas et al., 2007). During post-bloom, oligotrophic conditions, however, small phytoplankton are expected to increase in relative abundance as a food source (Agawin et al., 2000; Calbet, 2001; Echevarria et al., 2009; Takahashi et al., 1975), forcing a shift in the zooplankton assemblage toward species of smaller size (Lochte et al., 1993; Sieracki et al., 1993; Steele and Frost, 1977; Vargas et al., 2007). These smaller animals are not included in the field data analysis by Lavaniegos and Ohman (2007), explaining in part why zooplankton biomass estimates in this data set dropped so drastically after the phytoplankton bloom period (Fig. 4 C).

The hypothesis is supported by microzooplankton biomass data acquired in April 2006, May 2007 and November 2008 offshore of Point Conception during the process cruises of the CCE-LTER Program (http://cce.lternet.edu/; Ohman, unpubl.; Landry, unpubl.). Comparing microzooplankton to macrozooplankton biomass, the ratio of micro:macro almost doubles between the bloom (April-May) and the non-bloom seasons (November), indicating the enhanced biomass contribution and role of smaller organisms during the second half of the year (Table 4).

In contrast to the field data, the modeled zooplankton compartment can be regarded as a closure term which includes parameterizations of both large and small forms, the latter feeding not only on phytoplankton but also on bacteria and detritus (see formulae in Appendix 1). The model may therefore more accurately represent total zooplankton biomass throughout the year independent of its size structure. During the bloom period, the good fit between the model and data is consistent with observations that the bulk zooplankton biomass is dominated by large species, while the larger simulated than observed biomass in the second half of the year is likely due to the underrepresentation of the smaller size classes in the field data.

4.2. Monthly vs. daily forcing

Differences in the model responses to forcing by the daily versus monthly time series of the CUI provide insight into the effect of high-frequency variability in wind stress on system response. SSA analyses indicate that both CUI forcings are composed of three basic signals: annual, semiannual and a low-frequency signal. These signals are exactly the same in the monthly and daily CUI time series, and the sum of the three components gives reconstructions that are also identical for both time series (same amplitude and frequency). The major difference between the reconstructed signals is that the three components represent nearly 93% of total variability for the monthly time series, but only 55% of total variability for the daily data. This means that the high-frequency variability contains about 45% of the energy of the daily series, but only 7% of the monthly values.

Using CUI forcing with daily variability yielded 4.9% higher phytoplankton biomass and 8.5% higher zooplankton biomass than the simulation forced by monthly CUI (Table 3). Daily forcing also gave

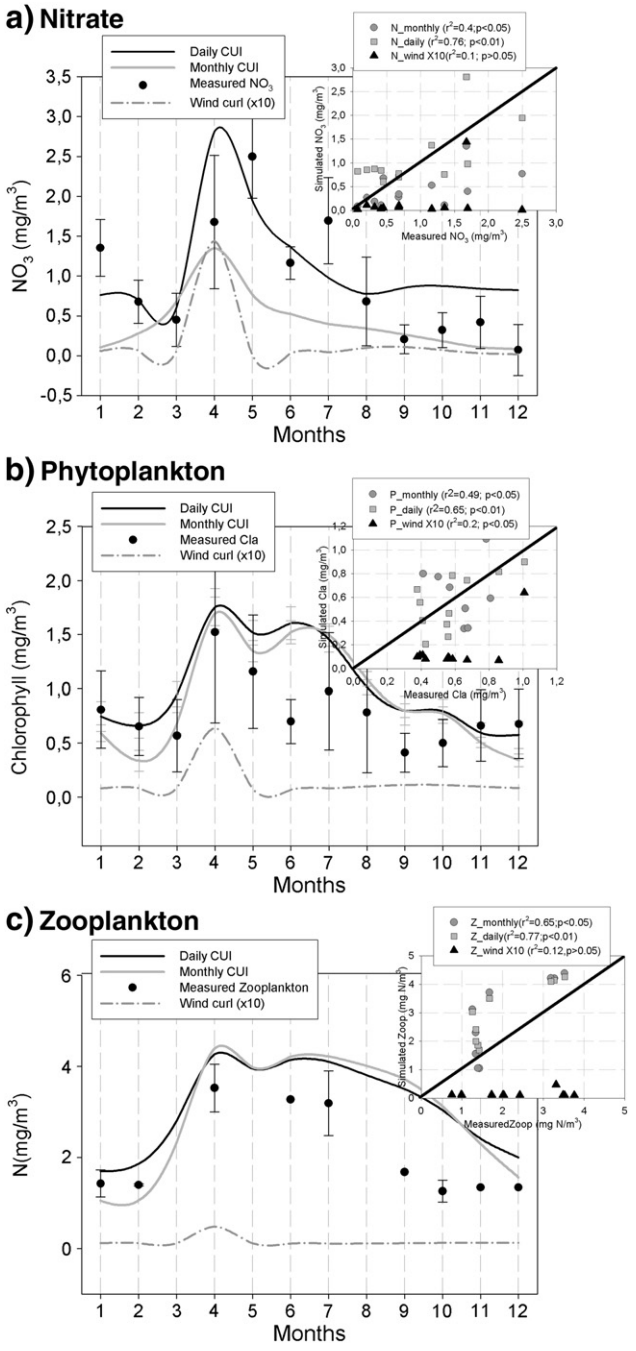

Fig. 4. Comparisons of climatological cycles of nitrate (a), phytoplankton biomass (b) and zooplankton biomass (c) in the observational data (black dots) and in the model forced by daily CUI (solid black line), monthly CUI (solid gray line) and wind curl (dashed black line). Insets in each figure show scatter plots between observations and model results: daily CUI (gray circles), monthly CUI (gray squares) and wind stress curl (black triangles).

the best fit to the field data (Fig. 4). This is consistent with the results of Gruber et al. (2006), who speculated that their model underestimated system chlorophyll because they used monthly means for the external forcing (upwelling and wind intensities), thereby missing the short-term variations typical of upwelling environments. Furthermore, Veneziani et al. (2009) found that realistic surface forcing was necessary to adequately represent the hydrographic spatial structure and temporal dynamics of the coastal CC region. This has also been suggested by Macías et al. (2010), who showed that the temporal dynamics of nutrient input can affect the total biomass produced by their effect on the matching of production-consumption cycles.

Yokomizo et al. (2010) used a conveyor-belt 1D model of the California coast, showing that short-scale interruptions of upwelling allowed more time for nutrient uptake to occur on the shelf, increasing the associated primary production in the region. The same explanation may be applied to our model even if space is not explicitly included. In our simulations, short-scale disruptions of the upwelling (including in the daily CUI data) also represent interruptions of the outflow from the modeled box (see model set-up description in M&M), thereby increasing the residence time of the water within this box. This should allow for more efficient nutrient incorporation and biomass accumulation than when those interruptions are eliminated from the CUI time-series (as in the monthly data).

4.3. Coastal upwelling vs. wind-stress curl-driven upwelling

How different processes contribute to the dynamics of the pelagic ecosystem in the SCCS is not entirely established. Early authors have viewed the inverse relationship between phytoplankton standing stock and the depth of the nitracline as an indication that regional primary production is largely determined by vertical advection and mixing of nitrate to the euphotic zone (Eppley and Holm-Hansen, 1986; Eppley et al., 1990; see also Aksnes et al., 2007). Our results tend to support this perspective, suggesting that the dynamics of the pelagic ecosystem are mainly driven by the magnitude and strength of coastal upwelling. However, coastal upwelling only can regulate the nitrate delivery that underlies phytoplankton and zooplankton dynamics in the northeastern coastal region of the bight, not in the offshore areas (Fig. 5).

More recent observations have found no correlations between either remotely sensed chlorophyll data (Legaard and Thomas, 2006; Santoro et al., 2010) or in situ chlorophyll measurements (Kim et al., 2009) and local winds or SST. This has led to the alternative view that coastal upwelling is not the dominant forcing mechanism in the SCCS. However, production in the deeper euphotic zone (invisible to satellites) could be responsible for much of the wind-forced variability in primary and secondary production in the region, leading to the lack of correlation between wind and satellite-derived production estimations reported previously. Similarly, the in situ chlorophyll data used by Kim et al. (2009) to compare with wind forcing were from the Scripps Pier, an extremely shallow nearshore location more likely affected by local tidal dynamics, swell and other processes than by regional winds.

Although much weaker than coastal upwelling on an areal basis, upwelling induced by wind-stress curl is a potentially important source of nutrients to offshore surface waters, which comprise a large area of the SCCS (Rykaczewski and Checkley, 2008). The present model suggests that the amount of nutrients introduced into the surface layer (and consequently the induced phytoplankton and zooplankton biomass) by the wind curl is roughly one tenth that of coastal upwelling (Fig. 4), in good agreement with some previous reports (e.g., Schwing et al., 1996). This is, however, a likely underestimate of the importance of wind-curl upwelling because we forced the model with winds that were very coarsely resolved in space and time. Recent estimates of wind-stress curl-induced upwelling based on high-resolution winds (Pickett and Paduan, 2003) and mooring data (Dever et al., 2006) have shown that it could be similar in magnitude to the coastal upwelling in some regions of the CC.

Despite the low absolute value of wind-stress curl-induced upwelling in our model, we observe a clear seasonality corresponding to the spring intensification of winds in the region (Mendelssohn and Schwing, 2002; Murphree et al., 2003). This intensification is in phase with changes in coastal upwelling (Fig. 4), with both mechanisms working in synchrony to bring nutrients to the surface layer.

4.4. Interannual variability and remote forcing

The model implementation allowed exploration of the mean or climatological state of the system and how the ecosystem responds to

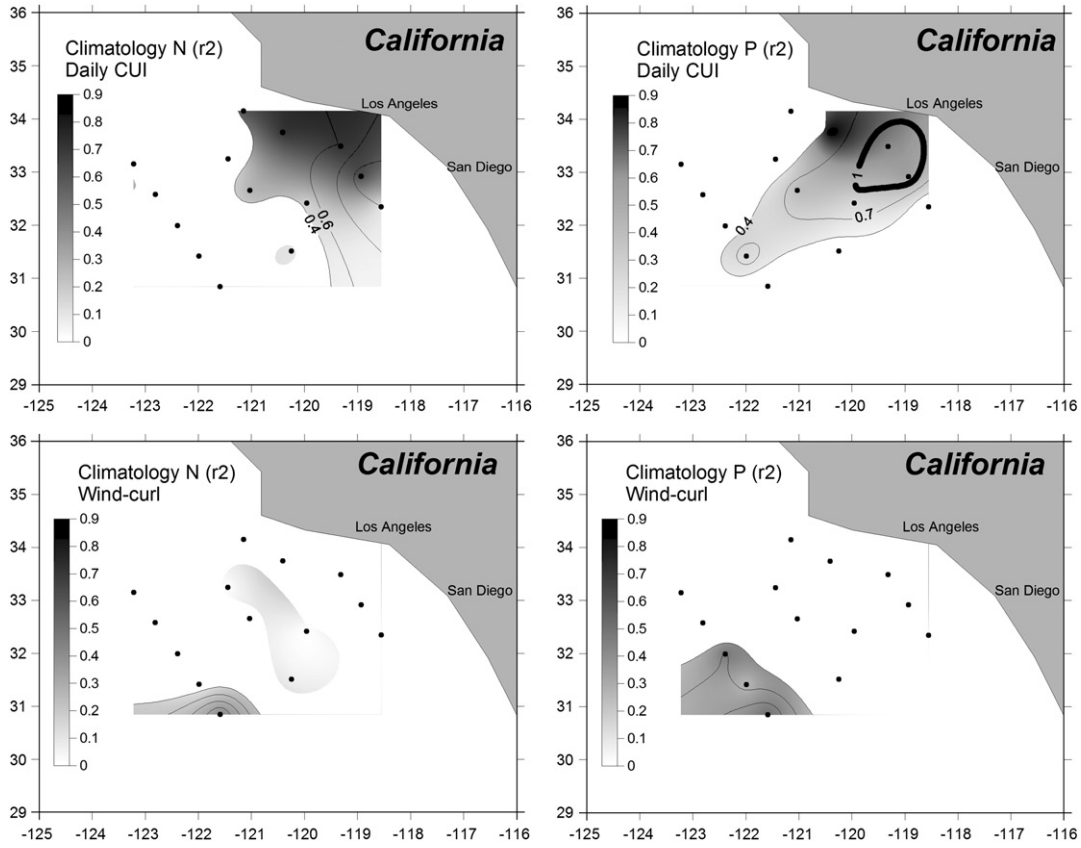

Fig. 5. Spatial patterns of correlation coefficients (background shading) and regression slopes (isopleths) between observed and modeled nitrate concentrations (left panels) and observed and modeled phytoplankton biomass (right panels). Upper panels are for comparisons to the model forced by daily CUI, and lower panels for wind stress curl-driven upwelling simulations.

isolated periods of perturbed forcing (Fig. 6). While the model was able to reproduce system behavior in the absence of major climatic perturbations (left panels Fig. 6), it was no able to replicate observed ecosystem responses to strong El Niño events such as seen during 1997–1998 (Bograd and Lynn, 2001) when most of the correlation between model and data disappeared (central panel of Fig. 6). An important effects of El Niño events in the region is the northward propagation of Kelvin waves from the equator, which lead to warmer and saltier waters in the coastal area off California (Enfield and Allen, 1980; Huyer and Smith, 1985). During 1997–1998, these waves deepened the thermocline (and nitracline) and raised sea level along the North American coast, resulting in decreased primary production and the lowest chlorophyll concentrations on record (Chavez et al., 1998, 1999; Kahru and Mitchell, 2000). This was followed by a period of increased cross-shore gradients in dynamic height, a significant shoaling of the nitracline, and a dramatic rebound in primary and secondary production, leading to the most extensive phytoplankton bloom ever observed in the equatorial Pacific (Chavez et al., 1999). These observations indicate that marine productivity can be controlled by large-scale remote forcing. The 0-D model implemented here with a constant 60 m base to the upper mixed layer cannot account for changing nutricline depths as occurred during the El Nino. Thus, it is not surprising that the ecosystem in the model did not respond as it did in situ.

In contrast to ENSO, the model-data correlations are not strongly affected by shifts in sign of the NPGO. The correlation distributions are, in fact, quite similar during the positive and negative phases of this climatic index (right and left panels of Fig. 6). However, maximum phytoplankton biomass predicted by the model during the negative phase of the NPGO are on average 24% lower than those during positive phase, corresponding to a weakening of coastal upwelling intensity.

As pointed out by Di Lorenzo et al. (2008), the NPGO is highly correlated with upwelling intensity and primary production in the CCE. Thus changes in the NPGO may already be included in the CUI fluctuations that force the model. Indeed, CUI values were significantly higher during the positive NPGO period (t-test, p-value$<$0.001). The fact that the model demonstrates equal skill in predicting biomass patterns during negative and positive phases of this climatic index (Fig. 6) seems to confirm that control of primary production by the NPGO cycles is mainly done through modification of the intensity of upwelling favorable winds.

5. Conclusions

We have presented a simple wind-forced physical-biological model that gives statistically significant simulations of the basic annual cycles of nitrate, phyto- and zooplankton in the Southern California Current ecosystem. Scaling the phytoplankton growth rate parameterization to experimentally measured field rates markedly improved the model's representation of nitrate concentration. Forcing the model with daily variability in upwelling favorable winds (CUI) also enhanced the fit between simulations and data relative to monthly mean wind forcing, demonstrating the importance of high-frequency wind variability in modulating the system dynamics. Upwelling due to wind-stress curl induced one order of magnitude less biomass than did coastal upwelling. However, wind-stress curl-induced upwelling was likely underestimated in the model due to poor resolution of the wind gradients. Importantly, wind-stress curl upwelling occurred synchronously with coastal upwelling, extending nutrient enrichment to the offshore. Finally, the model indicated that NPGO remote forcing of production patterns occurs through modifications of upwelling activity, by

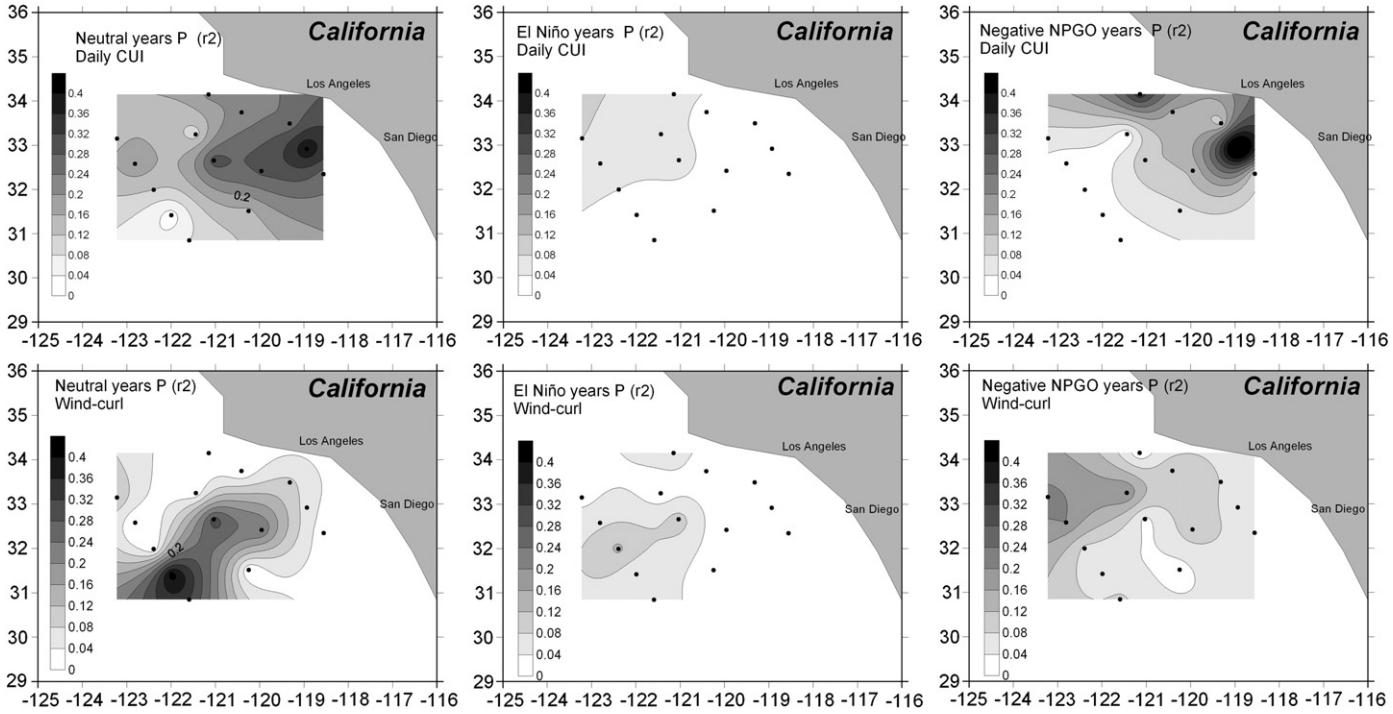

Fig. 6. Distributions of correlation coefficients comparing phytoplankton observations and simulations during 'neutral' years (2000–2004, left panels), 'El Niño' years (1995–1999, central panels) and negative NPGO years (1993–1994, left panels). Model forcing is by daily CUI (upper panels) and wind-curl upwelling (lower panels).

Table 4
Ratio microzooplankton:macrozooplankton biomass in the different CCE-LTER process cruises offshore of Point Conception.

Cruise name	Date	Micro:Macro
LTER-P0704	April 2007	1.01
LTER -P0605	May 2006	1.34
LTER-P0810	October 2008	2.47

affecting the intensity of the along-shore winds, while El Niño effects are more related to changes in surface water mass properties, some of which are caused by remote forcing not considered by this model. Consequently, NPGO effects are well represented in the wind-forced model, but the model does a poor job when simulating the effects of ENSO perturbations.

Acknowledgements

D.M. was funded by a postdoctoral contract by the Spanish Ministry of Science (contract nº EX2008-0394). This work was supported by National Science Foundation funding (OCE 04-17616 and OCE 10-266607) for the California Current Ecosystem LTER site. We thank two anonymous reviewers for their comments on earlier versions of the manuscript and E. Hoffman for efficiently handling the revision as editor.

Appendix 1. Biogeochemical model equations

Phytoplankton:

$$\frac{dP}{dt} = ((1-\Omega) * J * Q * P) - G_1 - m_1) - P * \left(\frac{flux}{Vt}\right); \tag{A.1}$$

Where:

$$J = \left(\frac{\log\left(\sqrt{(I_0 * \lambda)^2 * \alpha^2} + \sqrt{Vp^2 + ((I_0 * \lambda)^2 * \alpha^2)}\right) * (Vp * \alpha * (I_0 * \lambda))}{\sqrt{(I_0 * \lambda)^2 * \alpha^2} * ((k_w + (k_c * P))} \right. \tag{A.2}$$

$$\left. - \frac{\log\left(\left(\sqrt{(I_0 * \lambda)^2} * e^{-((k_w + (k_c * P)) * Depth)}\right) + \sqrt{Vp^2 + \left((I_0 * \lambda)^2 * \alpha^2 * e^{-((k_w + (k_c * P)) * Depth)^2}\right)}\right) * (Vp * \alpha * (I_0 * \lambda))}{\sqrt{(I_0 * \lambda)^2 * \alpha^2} * ((k_w + (k_c * P))} \right) / Depth;$$

Where:

$$V_p = \left(\frac{1}{3.7}\right) * \left(0.6 * \left(1.066^T\right)\right) \tag{A.3}$$

T in °C

$$Q = Q_1 + Q_2; \tag{A.4}$$

being:

$$Q_1 = N_n \frac{e^{-psi*N_r}}{(k_1 + N_n)}; \tag{A.5}$$

and

$$Q_2 = \frac{N_r}{(k_2 + N_r)}; \tag{A.6}$$

$$G_1 = \frac{g * Z * p_1 * P^2}{k_3 * F + F2}; \tag{A.7}$$

being:

$$F = (p_1 * P) + (p_2 * B) + (p_3 * D); \tag{A.8}$$

and

$$F2 = \left(p_1 * P^2\right) + \left(p_2 * B^2\right) + \left(p_3 * D^2\right); \tag{A.9}$$

$$m_1 = mu_1 * \frac{P^2}{(k_5 + P)}; \tag{A.10}$$

And ***flux*** refers to the incoming/outcoming water flux to the simulated box while ***Vt*** is the total volume of the simulated box.

Zooplankton:

$$\frac{dZ}{dt} = (\beta * (G_1 + G_2 + G_3) - m_2 - m_5) - Z * \left(\frac{flux}{Vt}\right); \tag{A.11}$$

Where:

G_1 = defined above;

$$G_2 = \frac{g * Z * p_2 * B^2}{k_3 * F + F2}; \tag{A.12}$$

$$G_3 = \frac{g * Z * p_3 * D^2}{k_3 * F + F2}; \tag{A.13}$$

$$m_2 = mu_2 * Z; \tag{A.14}$$

$$m_5 = mu_5 * Z^2; \tag{A.15}$$

Bacteria:

$$\frac{dB}{dt} = (U_1 + U_2 - G_2 - m_3) - B * \left(\frac{flux}{Vt}\right); \tag{A.16}$$

Where:

$$U_1 = B * \frac{Vb * Nd}{k_4 + S + Nd}; \tag{A.17}$$

$$U_2 = B * \frac{Vb * S}{k_4 + S + Nd}; \tag{A.18}$$

being:

$$S = \min(Nr, nu * Nd); \tag{A.19}$$

G_2 = defined above;

$$m_3 = mu_3 * B; \tag{A.20}$$

Detritus:

$$\frac{dD}{dt} = ((1-\beta) * (G_1 + G_2) - \beta * G_3 - m_4 + m_1) - D * \left(\frac{flux}{Vt}\right) * \left(\frac{S_D}{Depth}\right); \quad (A.21)$$

Where:

$$m_4 = mu_4 * D; \quad (A.22)$$

And all other parameters have been described elsewhere.
Nitrate:

$$\frac{dNn}{dt} = -(J * Q_1 * P) + \left(in\_Nn - Nn\right) * \left(\frac{flux}{Vt}\right); \quad (A.23)$$

Where:

in_Nn is the nitrate concentration in the incoming flux (i.e. the deep waters nitrate concentration).

Ammonium:

$$\frac{dNr}{dt} = -(J * Q_2 * P) - U_2 + m_3 + (1-\delta) * m_2 - Nr * \left(\frac{flux}{Vt}\right); \quad (A.24)$$

Dissolved Organic Nitrogen (DON):

$$\frac{dNd}{dt} = -U_1 + (\gamma * J * Q * P) + m_4 + (\delta * m_2) - Nd * \left(\frac{flux}{Vt}\right); \quad (A.25)$$

References

Agawin, N.S.R., Duarte, C.M., Agustí, S., 2000. Nutrient and temperature control of the contributions of picoplankton to phytoplankton biomass and production. Limnol. Oceanogr. 45 (3), 591–600.

Aksnes, D.L., Ohman, M.D., Rivis, D.L., 2007. Optical effect on the nitracline in a coastal upwelling area. Limnol. Oceanogr. 52, 1179–1187.

Allen, J.S., 1941. Ocean pasturage in California waters. Sci. Mon. LII, 261–264.

Allen, J.S., 1980. Models of wind-driven currents on the Continental Shelf. Annu. Rev. Fluid Mech. 12, 389–433.

Atlas, E.L., Hager, S.W., Gordos, L.I., Park, P.K., 1971. A practical manual for use of the Technicon AutoAnalyzer in sea-water nutrient analyses, revised, Deep oceanography. Oregon State University. 49 pp.

Bakun, A., 1973. Coastal upwelling indices, west coast of North America, 1946–1971. NOAA Technical Repport NMFS SSRF-671. U.S. Department of Commerce, Washington, DC.

Bograd, S.J., Lynn, R.J., 2001. Physical-biological coupling in the California Current during the 1997–99 El Niño-La Niña cycle. Geophys. Res. Lett. 28 (2), 275–278.

Bograd, S.J., Checkley, D.A., Wooster, W.S., 2003. CalCOFI: a halfcentury ofphysical, chemical, and biological research in the California Current System. Deep-Sea Res. Part II 50, 2349–2353.

Brock, T.D., 1981. Calculating solar radiation for ecological studies. Ecol. Model. 14, 1–19.

Calbet, A., 2001. Mesozooplankton grazing effect on primary production: A global comparative analysis in marine ecosystems. Limnol. Oceanogr. 46 (7), 1824–1830.

Carr, M.E., 2002. Estimation of the potential productivity in Eastern Boundary Currents using remote sensing. Deep-Sea Res. Part II 49, 59–80.

Castro, C.G., Collins, C.A., Walz, P., Pennington, J.T., Michisaki, R.P., Friederich, G., Chavez, F.P., 2002. Nutrient variability during El Niño 1997–98 in the California current system off central California. Prog. Oceanogr. 54, 171–184.

Chavez, F.P., Strutton, P.G., McPhaden, M.J., 1998. Biological-physical coupling in the central equatorial Pacific during the onset of the 1997–98 El Niño. Geophys. Res. Lett. 25 (19), 3543–3546.

Chavez, F.P., Strutton, P.G., Friedrich, G.E., Feely, R.A., Feldman, G.C., Foley, D.G., McPhaden, M.J., 1999. Biological and chemical response of the equatorial Pacific Ocean to the 1997–98 El Niño. Science 286, 2126–2131.

Dever, E.P., Dorman, C.E., Largier, J.L., 2006. Surface boundary-layer variability off Northern California, USA, during upwelling. Deep-Sea Res. Part II 53, 2887–2905.

Di Lorenzo, E., 2003. Seasonal dynamics of the surface circulation in the Southern California Current System. Deep-Sea Res. Part II 50, 2371–2388.

Di Lorenzo, E., Schneider, N., Cobb, K.M., Franks, P.J.S., Chhak, K., Miller, A.J., McWilliams, J.C., Bograd, S.J., Arango, H., Curchitser, E., Powell, T.M., Rivière, P., 2008. North Pacific Gyre Oscillation links ocean climate and ecosystem change. Geophys. Res. Lett. 35, L08607.

Echevarria, F., Zabala, L., Corzo, A., Navarro, G., Macías, D., Prieto, L., 2009. Spatial distribution of autotrophic picoplankton in relation to physical forcings: the Gulf of Cádiz, Strait of Gibraltar and Alborán Sea case study. J. Plankton Res. 33 (11), 1339–1351.

Enfield, D.B., Allen, J.S., 1980. On the structure and dynamics of monthly mean sea level anomalies along the Pacific coast of North and South America. J. Phys. Oceanogr. 10, 557–578.

Eppley, R.W., 1972. Temperature and phytoplankton growth in the sea. Fisheries Bulletin, US 70, 1063–1085.

Eppley, R.W., Holm-Hansen, O., 1986. Primary production in the Southern California Bight. In: Eppley, R.W. (Ed.), Plankton Dynamics in the Southern California Bight, pp. 176–209.

Eppley, R.W., Rogers, J.N., McCarthy, J.J., 1969. Half saturation constrats for uptake of nitrate and ammonium by marine phytoplankton. Limnol. Oceanogr. 14, 912–920.

Eppley, R.W., Garside, C., Renger, E.H., Orellana, E., 1990. Variability of nitrate concentration in nitrogen-depleted subtropical surface waters. Mar. Biol. 107, 53–60.

Fasham, M.J.R., 1995. Variations in the seasonal cycle of biological production in subarctic oceans: A model sensitivity analysis. Deep-Sea Res. 42, 1111–1149.

Fasham, M.J.R., Ducklow, H.W., McKelvie, S.M., 1990. A nitrogen-based model of plankton dynamics in the oceanic mixed layer. J. Mar. Res. 48, 591–639.

Fasham, M.J.R., Sarmiento, J.L., Slater, R.D., Ducklow, H.W., Williams, R., 1993. Ecosystem behaviour at Bermuda Station "S" and Ocean Weather Station "India": a general circulation model and observational analysis. Global Biochemical Cycles 2 (2), 379–415.

Fennel, K., Wilkin, J., Levin, J., Moisan, J., O'Reilly, J., Haidvogel, D., 2006. Nitrogen cycling in the Middle Atlantic Bight: Results from a three-dimensional model and implications for the North Atlantic nitrogen budget. Glob. Biochem. Cycles 20, GB3007. doi:10.1029/2005 GB002456.

Franks, P.J.S., 1992. Sink or swim:accumulation of biomass at fronts. Mar. Ecol. Prog. Ser. 82, 1–12.

Geider, R.J., MacIntyre, H.L., Kana, T.M., 1998. A dynamic regulatory model of phytoplanktonic acclimation to light, nutrients, and temperature. Limnol. Oceanogr. 43 (4), 679–694.

Gordon, L.I., Jennings, J.C., Ross, A.A., Krest, J.M., 1993. A suggested protocol for continuous automated analysis of seawater nutrients (phosphate, nitrate, nitrite and silicic acid) in the WOCE Hydrographic program and the Joint Global Ocean Fluxes Study, WOCE Operations Manual, vol. 3: The Observational Programme, Section 3.2: WOCE Hydrographic Programme, Part 3.1.3: WHP Operations and Methods. WHP Office Report WHPO 91–1; WOCE Report No. 68/91. November, 1994, Revision 1, Woods Hole, Mass., USA, 52 loose-leaf pages.

Gruber, N., Frenzel, H., Doney, S.C., Marchesiello, P., McWilliams, J.C., Moisan, J.R., Oram, J.J., Plattner, G.C., Stolzenbach, K.D., 2006. Eddy-resolving simulation of plankton ecosystem dynamics in the California Current System. Deep-Sea Res. Part I 53, 1483–1516.

Hayward, T.L., Venrick, E.L., 1998. Nearsurface pattern in the California Current: Coupling between physical and biological structure. Deep-Sea Res. 45, 1617–1638.
Henson, S.A., Thomas, A.C., 2007. Phytoplankton scales of variability in the California Current System: 1. Interannual and cross-shelf variability. J. Geophys. Res. 112, C07017. doi:10.1029/2006JC004039.
Hickey, B.M., 1979. The California Current System- hypotheses and facts. Prog. Oceanogr. 191–279.
Hickey, B.M., Banas, N.S., 2008. Why is the Northern End of the California Current System so Productive? Oceanography 21 (4), 90–105.
Hopkinson, B.M., Barbeau, K.A., 2008. Interactive influences of iron and light limitation on phytoplankton at subsurface chlorophyll maxima in the eastern North Pacific. Limnol. Oceanogr. 53 (4), 1303–1318.
Huyer, A., Smith, R.L., 1985. The signature of El Niño off Oregon in 1982–83. J. Geophys. Res. 90, 7133–7142.
Ianson, D., Allen, S.E., 2002. A two-dimensional nitrogen and carbon flux model in a coastal upwelling region. Glob. Biochem. Cycles 16 (1), 1011. doi:10.1029/2001GB001451.
Kahru, M., Mitchell, B.G., 2000. Influence of the 1997–98 El Niño on the surface chlorophyll in the California Current. Geophys. Res. Lett. 27, 2.937–2.940.
Kim, H., Miller, A.J., McGowan, J., Carter, M.L., 2009. Coastal phytoplankton blooms in the Southern California Bight. Prog. Oceanogr. 82, 139–147.
King, A.L., Barbeau, K., 2007. Evidence for phytoplankton iron limitation in the southern California Current System. Mar. Ecol. Prog. Ser. 342, 91–103.
Kistler, R.K.E., Collins, W., Saha, S., White, G., Woollen, J., Chelliah, M., Ebisuzaki, W., Kanamitsu, M., Kousky, V., Van der Dool, H., Jenne, R., Fiorino, M., 2001. The NCEP-NCAR 50 year Reanalysis: Monthly Means CD-ROM and documentation. Bull. Am. Meteorol. Soc. 82, 247–267.
Landry, M.R., Ohman, M.D., Goericke, R., Stukel, M.R., Tsyrklevich, K., 2009. Lagrangian studies of phytoplankton growth and grazing relationships in a coastal upwelling ecosystem off Southern California. Prog. Oceanogr. 83, 208–216.
Lavaniegos, B.E., Ohman, M.D., 2007. Coherence of long-term variations of zooplankton in two sectors of the California Current System. Prog. Oceanogr. 75, 42–69.
Laws, E.A., Bannister, T.T., 1980. Nutrient and light limited growth of Thalassiosira fluvialitis in continous culture, with implications for phytoplankton growth in the ocean. Limnol. Oceanogr. 25 (3), 457–473.
Legaard, K.R., Thomas, A.C., 2006. Spatial patterns in seasonal and interannual variability of chlorophyll and sea surface temperature in the California Current. J. Geophys. Res. 111, C06032. doi:10.1029/2005JC003282.
Li, Q.P., Franks, P.J.S., Landry, M.R., Goericke, R., Taylor, A.G., 2010. Modeling phytoplankton growth rates and chlorophyll to carbon ratios in California coastal and pelagic ecosystems. J. Geophys. Res. 115, G04003. doi:10.1029/2009JG001111.
Lochte, K., Ducklow, H.W., Fasham, M.J.R., Stienen, C., 1993. Plankton succession and carbon cycling at 47°N 20°W during the JGOFS North Atlantic Bloom Experiment. Deep-Sea Res. Part II 40 (1–2), 91–114.
Lynn, R.J., Simpson, J.J., 1987. The flow of the undercurrent over the continental borderland off southern California. J. Geophys. Res. 95 (12), 12995–13008.
Macías, D., Navarro, G., Echevarría, F., García, C.M., Cueto, J.L., 2007. Phytoplankton pigment distribution in the north-western Alboran Sea and meteorological forcing: a remote sensing study. J. Mar. Res. 65 (4), 523–543.
Macías, D., Ramírez, E., García, C.M., 2010. Effect of nutrient input frequency on the structure and dynamics of the marine pelagic community. A modelling approach. J. Mar. Res. 68, 119–151.
Mackas, D.L., Peterson, W.T., Ohman, M.D., Lavaniegos, B.E., 2006. Zooplankton anomalies in the California Current system before and during the warm ocean conditions of 2005. Geophys. Res. Lett. 33, L22S07.
Mantua, N.J., Hare, S.J., Zhang, Y., Wallace, J.M., Francis, R.C., 1997. A Pacific Interdecadal Climate Oscillation with Impacts on Salmon Production. Bull. Am. Meteorol. Soc. 78, 1069–1079.
Mantyla, A.W., Bograd, S.J., Venrick, E.L., 2008. Patterns and controls of chlorophyll-a and primary productivity cycles in the Southern California Bight. J. Mar. Syst. 73, 48–60.
McGillicuddy Jr., D.J., Robinson, A.R., McCarthy, J.J., 1995. Couple physical and biological modeling of the spring bloom in the North Atlantic (I): model formulation and one dimensional bloom processes. Deep-Sea Res. 42, 1313–1357.
Mendelssohn, R., Schwing, F.B., 2002. Common and uncommon trends in SST and wind stress in the California and Peru–Chile current systems. Prog. Oceanogr. 53, 141–162.
Moisan, J.R., Miller, A.J., Di Lorenzo, E., Wilkin, J., 2004. Modeling and data assimilation. In: Miller, R.L., Castillo, C.E.D., McKee, B.A. (Eds.), Remote Sensing of Coastal Aquatic Environments. Springer, New York, pp. 229–257.
Moore, A.M., Arango, H.G., Di Lorenzo, E., Cornuelle, B.D., Miller, A.J., Nelson, D.J., 2004. A comprehensive ocean prediction and analysis system based on the tangent linear and adjoint components of a regional ocean model. Ocean Modell. 7, 227–258.
Murphree, T., Green-Jessen, P., Schwing, F.B., Bograd, S.J., 2003. The seasonal cycle of wind stress curl and its relationship to subsurface ocean temperature in the Northeast Pacific. Geophys. Res. Lett. 30 (9), 1469. doi:10.1029/2002GL016366.
Ohman, M.D., Hirche, H.J., 2001. Density-dependent mortality in an oceanic copepod population. Nature 412, 638–641.
Ohman, M.D., Wilkinson, J.R., 1989. Comparative Standing Stocks of Mesozooplankton and Macrozooplankton in the Southern Sector of the California Current System. Fish. Bull. US 87, 967–976.
Olivieri, R.A., Chavez, F.P., 2000. A model of plankton dynamics for the coastal upwelling system of Monterey Bay, California. Deep-Sea Res. Part II 47, 1077–1106.
Osborne, B.A., Geider, R.J., 1986. Effects of nitrate-nitrogen limitation on photosynthesis in the diatom Phaeoductylum tricornutum Bohlin (Bacillariophyceae). Plant Cell Environ. 9, 617–625.
Pickett, M.H., Paduan, J.D., 2003. Ekman transport and pumping in the California Current based on the U.S. Navy's high-resolution atmospheric model (COAMPS). J. Geophys. Res. 108 (C10), 3327. doi:10.1029/2003JC001902.
Popova, E.E., Fasham, M.J.R., Osipov, A.V., Ryabchenko, V.A., 1997. Chaotic behaviour of an ocean ecosystem model under seasonal external forcing. Journal of Plankton Research 19 (10), 1495–1515.
Rebstock, G.A., 2003. Long-term change and stability in the California Current System: lessons from CalCOFI and other long-term data sets. Deep-Sea Res. Part II 50, 2583–2594.
Redfield, A.C., 1934. On the proportions of organic derivations in sea water and their relation to the composition of plankton. In: Daniel, R.J. (Ed.), James Johnstone Memorial Volume. University Press of Liverpool, pp. 177–192.
Riley, G.A., 1941. Plankton studies III. Long Island Sound. Bull. Bingham Oceanogr. Coll. 1–93 Art. III.
Rykaczewski, R.R., Checkley, D.M., 2008. Influence of ocean winds on the pelagic ecosystem in upwelling regions. PNAS 105 (6), 1065–1970.
Santoro, A.E., Nidzieko, N.J., van Dijken, G.L., Arrigo, K.R., Boehma, A.B., 2010. Contrasting spring and summer phytoplankton dynamics in the nearshore Southern California Bight. Limnol. Oceanogr. 55 (1), 264–278.
Sarmiento, J.L., Slater, R.D., Fasham, M.J.R., Ducklow, H.W., Toggweiler, J.R., Evans, G.T., 1993. A seasonal three-dimensional ecosystem model of nitrogen cycling in the North Atlantic euphotic zone. Glob. Biochem. Cycles 7, 417–450.
Schwing, F.B., Mendelssohn, R., 1997. Increased coastal upwelling in the California Current System. J. Geophys. Res. 102 (C2), 3421–3438.
Schwing, F.B., O'Farrell, M., Steger, J.M., Baltz, K., 1996. Coastal upwelling indices, west coast of North America, 1946–95. U.S. Dep. Commer.,NOAA Tech. Mem. NOAA-TM-NMFS-SWFSC-231.
Sieracki, M.E., Verity, P.G., Stoecker, D.K., 1993. Plankton community response to sequential silicate and nitrate depletion during the 1989 North Atlantic spring bloom. Deep-Sea Res. Part II 40 (1–2), 213–225.
Smith, R.L., 1968. Upwelling. Oceanogr. Mar. Biol. Annu. Rev. 6, 11–46.
Smith, S.D., Dobson, F.W., 1984. The heat budget at ocean station Bravo. Atmos. Oceanogr. 22, 1–22.
Smith, R.L., Huyer, A., Fleischbein, J., 2001. The coastal ocean off Oregon from 1961 to 2000: is there evidence of climate change or only of Los Niños? Prog. Oceanogr. 49, 63–93.
Steele, J.H., Frost, B.W., 1977. The Structure of Plankton Communities. Philos. Trans. R. Soc. Lond. 280, 485–534.
Steele, J.H., Henderson, E.W., 1981. A simple plankton model. Am. Nat. 117, 676–691.
Steele, J.H., Henderson, E.W., 1992. The role of predation in plankton models. J. Plankton Res. 14, 157–172.
Strub, P.T., James, C., 2000. Altimeter-derived variability of surface velocities in the California Current System: 2. Seasonal circulation and eddy statistics. Deep-Sea Res. Part II 47, 831–870.
Takahashi, M., Thomas, W.H., Siebert, D.L.R., Beers, J., Koeller, P., Parson, T.R., 1975. The replication of biological events in enclosed water columns. Arch. Hydrobiol. 76 (1), 5–23.
Thomas, A.C., Brickley, P., Weatherbee, R., 2009. Interannual variability in chlorophyll concentrations in the Humboldt and California Current Syst. Prog. Oceanogr. 83, 386–392.
Toggweiler, J.R., Carson, S., 1995. What are upwelling systems contributing to the ocean's carbon and nutrient budgets? Upwelling in the Ocean: Modern Processes and Ancient Records. John Wiley & Sons, Chichester, UK, pp. 337–360.
Vargas, C.A., Martínez, R.A., Cuevas, L.A., Pavez, M.A., Cartes, C., González, H.E., Escribano, R., Danieri, G., 2007. The relative importance of microbial and classical food webs in a highly productive coastal upwelling area. Limnol. Oceanogr. 52 (4), 1495–1510.
Veneziani, M., Edwards, C.A., Moore, A.M., 2009. A central California coastal ocean modeling study: 2. Adjoint sensitivities to local and remote forcing mechanisms. J. Geophys. Res. 114, C04020. doi:10.1029/2008JC004775.
Wainwright, T.C., Feinberg, L.R., Hooff, R.C., Peterson, W.T., 2007. A comparison of two lower trophic models for the California Current System. Ecol. Model. 202, 120–131.
Wooster, W.S., Reid, J.L., 1963. Eastern boundary currents, The Sea. Ideas and observations on progress in the study of the seas. John Wiley & Sons, Interscience Publishers, London & New York, pp. 253–280.
Yokomizo, H., Botsford, L.W., Holland, M.D., Lawrence, C.A., Hastings, A., 2010. Optimal wind patterns for biological production in shelf ecosystems driven by coastal upwelling. Theory Ecol. 3, 53–63.